

Performance Enhanced Ultrasound Probe Tracking with a Hemispherical Marker Rigid Body

Qianqian Cai, *Student Member, IEEE*, Chang Peng, *Member, IEEE*, Jian-yu Lu, *Fellow, IEEE*, Juan C. Prieto, Alan J. Rosenbaum, Jeffrey S. A. Stringer, and Xiaoning Jiang, *Senior Member, IEEE*

Abstract—Among tracking techniques applied in the 3D freehand ultrasound, the camera-based tracking method is relatively mature and reliable. However, constrained by manufactured marker rigid bodies, the ultrasound probe is usually limited to operate within a narrow rotational range before occlusion issues affect accurate and robust tracking performance. Thus, this study proposed a hemispherical marker rigid body to hold passive non-coplanar markers so that the markers could be identified by the camera, mitigating self-occlusion. The enlarged rotational range provides greater freedom for sonographers while performing examinations. The single-axis rotational and translational tracking performance of the system, equipped with the newly designed marker rigid body, were investigated and evaluated. Tracking with the designed marker rigid body achieved high tracking accuracy with 0.57° for the single-axis rotation and 0.01 mm for the single-axis translation for sensor distance between 1.5-2 m. In addition to maintaining high accuracy, the system also possessed an enhanced ability to capture over 99.76% of the motion data in the experiments. The results demonstrated that with the designed marker rigid body, the missing data was remarkably reduced from over 15% to less than 0.5%, which enables interpolation in the data post-processing. An imaging test was further conducted, and the volume reconstruction of a 4-month fetal phantom was demonstrated using the motion data obtained from the tracking system.

Index Terms—Ultrasound probe tracking, occlusion, marker configuration, 3D freehand ultrasound.

I. INTRODUCTION

A. Background

FOR decades, ultrasound (US) has been one of the common tools for nondestructive testing [1] and medical imaging [2]. It produces real-time images of structures within the human body or movement of internal organs by transmitting and receiving ultrasonic waves from ultrasonic transducers. Two-dimensional images are then reconstructed by a computer based on the echo signals. This imaging process is non-ionizing, which is preferred when radiation-sensitivity is a concern, such as for obstetrics [3]. Apart from being a non-invasive modality, US imaging is also portable, easily accessible, and cost effective. However, barriers exist in the

widespread clinical applications of US imaging since the image quality is highly dependent on sonographers' skills, knowledge and experience [2]. Furthermore, due to the limited field of view, multiple frames are often required to cover the whole scanning region, which makes it more challenging for sonographers to imagine the 3D view of an anatomical structure from a series of 2D images [4].

B. 3D US Imaging Techniques

3D freehand US imaging has been proposed to overcome the above limitations [5]. Current 3D US imaging methods can be categorized into three different types: mechanical scanning [6]–[8], 2D array scanning [9]–[11], and freehand scanning [12]–[16]. In mechanical scanning, the US probe is attached to a six degree-of-freedom robotic arm for scanning. The position and orientation of the probe can be accurately calculated based on the geometry of the robotic arm and the encoder information. However, the robot-assisted scanning system is usually too bulky and heavy to use in clinical applications [17]. In the 2D array scanning, the acoustic beams are steered electronically in both elevational and azimuthal directions to obtain a 3D view of the anatomy. It is the fastest way to view the real-time 3D images. However, the 2D array transducers are difficult to fabricate and thus usually comes with a high cost [18]. 3D freehand ultrasound scanning is a promising imaging modality, which can be realized with or without a tracking sensor. A sensorless freehand tracking estimates the position and orientation from the ultrasound images themselves. It does not require a complicated dependence of the scanning protocol. However, the speckle decorrelation typically requires fully developed speckles [19] and only partially captures the underlying complexity of ultrasound image formation [15]. It is especially challenging to accurately estimate the probe motion, particularly out-of-plane motion, as different image contents can be caused by the probe motion or different tissues. Also, the decorrelation rate depends not only on the transducers but also on the medium [15], [20]. Gee *et al.* [12] further extended the speckle decorrelation algorithms by adapting the decorrelation curves to account for apparent coherent scattering. Another challenge is how to eliminate the error accumulation between the two adjacent frames. A sensor-based 3D freehand ultrasound utilizes one or combinations of two or more of the following sensors: inertia sensors, acoustic sensors, electromagnetic sensors, and optical sensors. The inertial measurement unit (IMU) estimates position and orientation by taking integral of the acceleration and angular

This work was supported by Bill & Melinda Gates Foundation under the Award OPP1191684. (Corresponding author: Xiaoning Jiang.)

Q. Cai, C. Peng, and X. Jiang are with the Department of Mechanical and Aerospace Engineering, North Carolina State University, Raleigh, NC 27695, USA (e-mail: qcai2@ncsu.edu; cpeng6@ncsu.edu; xjiang5@ncsu.edu).

J. Lu is with Department of Bioengineering, University of Toledo, Toledo, OH 43606, USA (e-mail: jian-yu.lu@ieee.org).

J. Prieto, A. Rosenbaum, and J. Stringer are with Department of Obstetrics and Gynecology, University of North Carolina at Chapel Hill, Chapel Hill, NC 27599, USA (e-mail: juan_prieto@med.unc.edu; alan_rosenbaum@med.unc.edu; jeffrey_stringer@med.unc.edu)

velocities, respectively [21]. However, the positional tracking suffers from drifting [22]. A recent study by Prevost *et al.* [15] considered IMU sensors to be adequate for rotational tracking but insufficient for positional tracking due to their low signal-to-noise ratio and the required double integration. They turned out to achieve the 3D reconstruction of freehand ultrasound sweeps using a convolutional neural network with orientation data from an IMU sensor. Acoustic sensors solve the target positioning using the sound speed, receiver positions and measured time-of-flight or time-difference-of-flight [23]. Thus, it can be applied in dark environments such as in an ultrasound exam. However, to maintain a high signal-to-noise ratio, the tracking volume is limited. And there should not be any obstacles between the transmitters and the receivers [24]. Among all existing tracking techniques, optical tracking and electromagnetic tracking are more popular in the indoor environment, especially in clinical applications. In an obstetrical exam, large metal objects are usually inevitable. Therefore, Lang *et al.* [13] tried to fuse the speckle decorrelation method with the electromagnetic sensor to correct the metallic distortions of the electromagnetic sensor. Compared with electromagnetic tracking, optical tracking is more preferred in some cases. Optical tracking uses a camera system to determine the real-time position and orientation of an object either by tracking a set of markers or from RGB (red, green, and blue) images. The former uses a fixed camera system to track a set of active or passive infrared markers attached to the object. The latter is a mimic of human eyes that captures depths information from the RGB images [25]. Therefore, it requires a good illumination condition. In fetal ultrasound, the lighting is usually controlled by a combination lighting system (dim/bright). In most cases, the room is dark so that the sonographer can view the images clearly on the device's display. In situations like this, a camera system may struggle to capture useful RGB images to calculate the depth information. Therefore, optical tracking with infrared markers is more suitable. Active markers are battery powered and thus are usually heavier than passive markers [26]. To ensure continuous tracking during the operation, passive infrared (IR) markers were adopted in this research.

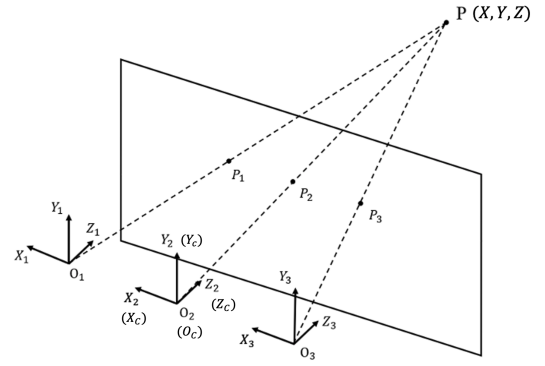
C. Objective

Although optical tracking is accurate, the tracking performance can be limited by occlusion, which is discussed in the following sections. The objective of this study is to improve the tracking performance of the camera-based tracking by replacing the 2D marker rigid body with a newly designed hemispherical marker rigid body. With most motion data captured, the occlusion issues can be mitigated. Thus, the reconstruction from 2D frames to 3D volume is expected to possess more motion information to reflect the structure of the imaging object.

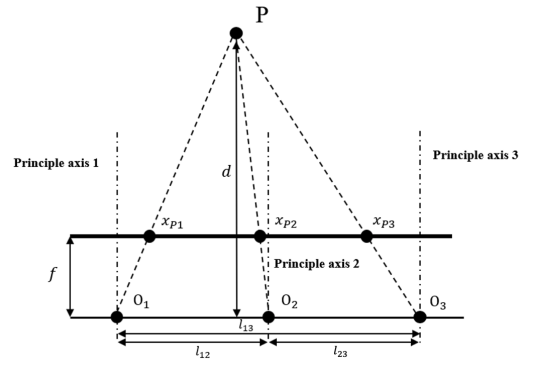
II. CAMERA-BASED TRACKING

A. Principle of Camera-Based Tracking

Theoretically, a point in the 3D space can be located by triangulation if it can be seen by two or more lenses simultaneously.



(a) Schematic of the camera-based tracking. The three coordinates represent the three lenses integrated in the camera bar. The reference coordinate $X_c Y_c Z_c$ coincides with the $X_2 Y_2 Z_2$. In the schematic, the camera bar is looking at point P, where P_1, P_2 , and P_3 are the intersections on the image plane.



(b) Schematic of the camera-based tracking. This top view demonstrates the similar triangles used to calculation the position information. The depth d of point P can be determined via triangulation.

Fig. 1. Principle of the optical tracking technique

Fig. 1(a) and Fig. 1(b) show the schematics of the tracking principle. O_1, O_2 , and O_3 are the origins of three lenses whose principal axes are parallel with each other. The line connecting each two of the three lenses is the baseline. The baseline is perpendicular to the principal axes. In this paper, the 3D world reference coordinate (C) was chosen to be the right-handed, y-up coordinate system, where the origin was set to coincide with the center of the cameras by default. The 2D marker position can be easily obtained in the image coordinate. Then, using 2D projection obtained from multiple lenses, the perception of the depth information could be estimated from the disparity of 3D points in the different images. For example, when a point P in the 3D space is viewed by the left two lenses, the position (X, Y, Z) could be calculated as follows [27].

$$\begin{aligned} Z &= \frac{f l_{12}}{x_{p1} - x_{p2}} \\ X &= \frac{x_{p1} Z}{f} \\ Y &= \frac{y_{p1} Z}{f} \end{aligned} \quad (1)$$

where f is the focal length of all the three cameras, l_{12} is the baseline between the first and the second lenses, and

$x_{p1} - x_{p2}$ is known as the disparity and represents how much the left image is displaced with respect to the right image. With markers' position known, the marker coordinate (M) associated with the rigid body created from the markers is also known. Therefore, the yaw (α), pitch (β), roll (γ) in the rotation matrix R can be deduced from the homogeneous transformation matrix T_M^C (representing the transformation from coordinate M to C) as below.

$$T_M^C = \begin{bmatrix} \mathbf{R} & \mathbf{p} \\ \mathbf{0} & 1 \end{bmatrix} \quad (2)$$

where

$$R = \begin{bmatrix} \cos\alpha\cos\beta & \cos\alpha\sin\beta\sin\gamma - \sin\alpha\cos\gamma \\ \sin\alpha\cos\beta & \sin\alpha\sin\beta\sin\gamma + \cos\alpha\cos\gamma \\ -\sin\beta & \cos\beta\sin\gamma \\ & \cos\alpha\sin\beta\cos\gamma + \sin\alpha\sin\gamma \\ & \sin\alpha\sin\beta\cos\gamma - \cos\alpha\sin\gamma \\ & \cos\beta\cos\gamma \end{bmatrix}$$

and

$$\mathbf{p} = (X_M, Y_M, Z_M)^T \\ \mathbf{0} = (0, 0, 0)$$

(X_M, Y_M, Z_M) is the origin of the marker coordinate M expressed in the reference coordinate C . With R_{ij} denoting the entry that lies in the row i and column j ($i, j \in \{1, 2, 3\}$), the orientation can then be obtained from the entries of the rotation matrix, where

$$\alpha = \arctan \frac{R_{12}}{R_{11}} \\ \beta = -\arcsin R_{31} \\ \gamma = \arctan \frac{R_{32}}{R_{33}} \quad (3)$$

Optical tracking systems using spherical markers coated with the infrared light retro-reflective material can achieve up to sub-millimeter tracking accuracy [16], [28]. The cable-free connection between the probe and the external tracking device allows for flexibility for the sonographers. It also has the potential to simultaneously track multiple targets, such as both the probe and the patient, in the event that the patient moves during the scanning.

B. Limitations of Camera-Based Tracking

One major disadvantage of camera-based tracking is that it requires direct line-of-sight, which is not possible if the object is out of the tracking volume [29], if there is occlusion [30], or if the markers are damaged [26]. In the application of the 3D freehand US imaging, stepping out of the tracking volume is usually not problematic given the large pyramid tracking volume (compared with the operation space) provided by an up-to-date optical tracking device such as the one shown in Fig. 2. A damaged marker may not be identified by the circle filter if there is damage on the retro-reflective surface resulting in not satisfying the user-defined brightness threshold. Therefore, during the operation and maintenance, operators are responsible for protecting the markers' surfaces, checking the

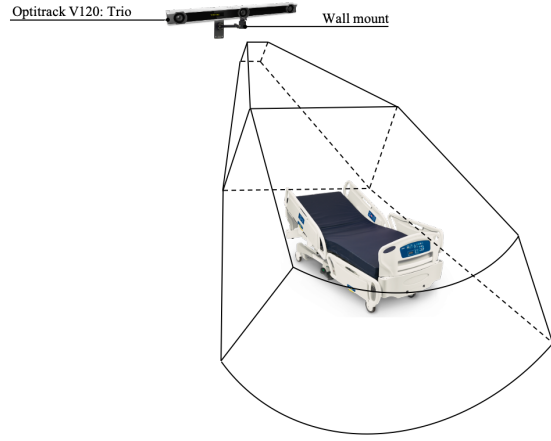


Fig. 2. Schematic of the tracking volume size of the Optitrack V120: Trio

markers' conditions, and replacing damaged markers before each use. Lastly, and most frequently, occlusion may occur, although its occurrence depends greatly upon target geometry, marker size, and camera setup [28]. Occlusion can be further divided into two categories: self-occlusion (where markers are hidden by other markers) background occlusion (where the marker rigid body is obscured by other objects).

To alleviate the occlusion, a multi-single-lens camera system may be adopted to ensure that the tracking volume is covered by multiple cameras arranged in different locations instead of an integrated camera bar [16]. This solution improves tracking robustness but introduces new challenges with installation, calibration, and cost. Given moderate probe motion in an US exam, the occlusion issues can instead be addressed by adopting a designed marker arrangement. In a 3D space, a minimum number of 3 markers are required to define a rigid body in space. Additional markers can increase the robustness by mitigating the likelihood of occlusion. Therefore, the marker rigid body usually consists of four or more markers. To avoid "flipping" during the tracking, the marker rigid body should be arranged asymmetrically.

III. MATERIALS AND METHODS

A. Marker Layout

In a previous study, we demonstrated submillimeter positional tracking accuracy and $<1^\circ$ orientational tracking with an optical system [31]. However, the maximum rotational range of the 2D marker rigid body was within 90° . If the US probe is operated out of this range, some of the markers may be hidden and therefore the entire rigid body cannot be identified by the camera, resulting in inaccurate tracking or failed tracking. Since rotation of a probe is not limited or predefined in a real US exam, we aimed to enable true unlimited freehand movement while retaining similar materials cost, using a hemispherical marker rigid body. A total of thirteen unoccupied holes were designed on the hemisphere to hold the rods attached with passive markers. One is centered at the top of the hemisphere; the others can be divided into four groups, with each three sharing the same radius and the same angle between the central axis of the hemisphere and the

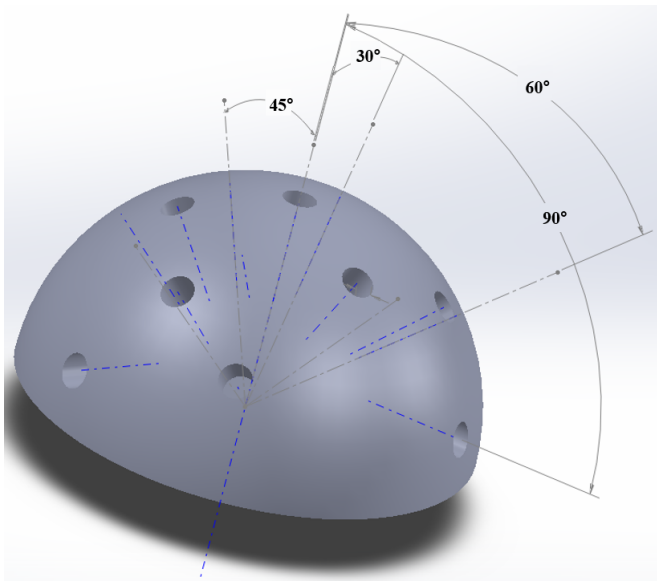


Fig. 3. Designed hemispherical rigid body to hold the passive markers and rigid rods

axis of the hole. Fig. 3 shows the 3D model of the designed rigid body with hole axes angled at 30° , 45° , 60° , and 90° . By choosing the target holes and proper rod lengths, the attached markers may be separated asymmetrically so that if any one marker was hidden or partially hidden by another marker, the remaining markers are still at a minimal distance of 10 ± 1 mm. In this way, the self-occlusion issue may be mitigated.

Five markers were attached to the marker rigid body with different rod lengths as shown in Fig. 4(b). Considering the general rotation of an object, the pointing angle was defined in a spherical region. During US exams, the US probe is typically rotated by the sonographer in the upper hemispherical region. Therefore, the rigid body was designed with a hemispherical surface superiorly to hold the markers and a circular bottom with a rigid rod to connect the marker rigid body with the probe. According to the characteristics of the probe rotation and the geometry of the rigid body, a marker that is inserted in the top hole with a certain rod length can be viewed by the camera most often and was thus considered the primary marker. To avoid the marker rigid body touching the patient's gravid abdomen during the operation, placing the markers on the top region of the rigid body rather than the side region is preferred. Therefore, the remaining markers were positioned in a descending spiral manner. Three markers occupied the three 30° -holes. Based upon the rules of minimizing occlusion and asymmetric arrangement, different rod lengths were selected experimentally so that the four markers were not coplanar within the camera's view. Rod lengths were selected for which the marker rigid body would not touch the patient's abdomen when rotated during the exam. With four markers inserted on the top region of the hemisphere, the final marker was located to locate at a 90° -hole, adding to the asymmetry and spreading the marker layout by increasing the Euclidean distance between markers to make the tracking more robust. The selected rod length for each of the markers attached

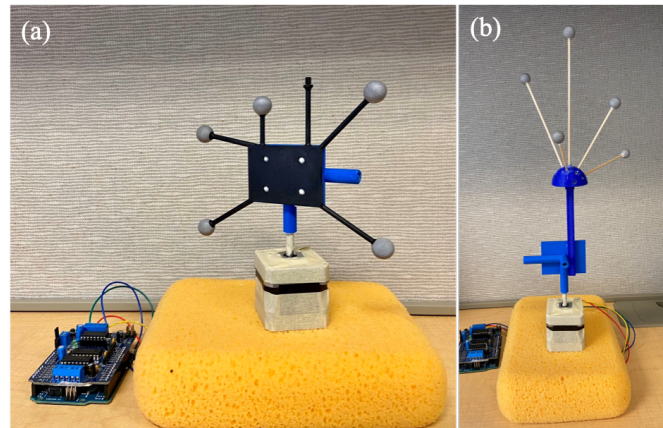


Fig. 4. Experiment setup for rotational test. (a) The 2D marker rigid body from the manufacture was attached to the stepper motor; (b) The designed hemispherical marker rigid body was attached to the stepper motor.

to the 3D hemispherical rigid body were 35.16 mm, 107.86 mm, 130.07 mm, 73.93 mm, and 84.58 mm. The resulting non-coplanar marker distribution is shown in Fig. 5. With this asymmetric marker distribution, the attached five markers were placed on concentric circles with different radii, ensuring proper distance between every two of the five markers so that none of the pair-wise markers were too close for the camera to detect.

B. Data Acquisition and Processing

1) *Rotational Tracking Performance*: A rotational tracking test was conducted to assess the tracking performance during the 360° rotational motion. The test setups are shown in Fig. 4. In the tests, the camera used for tracking the probe motion was OptiTrack V120: Trio (NaturalPoint, Inc.). With three lenses integrated, no calibration of the camera is required at the user end and the cost is relatively low compared with other commercial multi-single-lens camera systems. Both the 2D marker rigid body and the hemispherical marker rigid body were attached to a step motor that had 200 steps per revolution. To imitate the rotational speed during an US exam, the stepper motor was set to rotate at 3 rpm . Both marker sets were rotated 360° along each of the axis for 5 successive tests. Without loss of generality, each test started from a different initial orientation. The motion was captured by the camera at an update rate of 120 Hz. The accuracy was evaluated based on the totally recorded rotational angle and the difference between the initial and the final angle. For the recorded motion data, an ideal case was that the motion be accurately captured with no missing data. However, the occlusion is known as an inherent drawback of the optical tracking. Therefore, when occlusion happened, less missing data was better, serving as another criterion to evaluate the tracking quality. Missing entries were filled based upon its neighbours using the moving average. The window length was set to be 12 sample data points, which is equal to 0.1 second in time length, during which the probe can be considered still.

2) *Translational Tracking and Volume Reconstruction*: To validate volume reconstruction, a 3D printed phantom

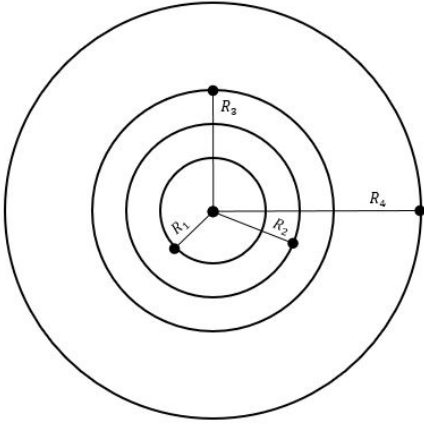


Fig. 5. Top view of the five markers' distribution located superiorly on the hemispherical marker rigid body shown in Fig. 4(b)

TABLE I

COMPARISON OF SINGLE-AXIS ROTATIONAL TRACKING PERFORMANCE

	Recorded Rotation ($^{\circ}$)		Difference ($^{\circ}$)	
	2D*	HS**	2D	HS
X-axis	359.1	359.8	-0.03	0
Y-axis	357.2	358.8	-0.008	0
Z-axis	N/A	359.7	N/A	0

* 2D: 2D marker rigid body

** HS: hemispherical marker rigid body

(Fig. 9(a)) was scanned with a Butterfly iQ probe (Butterfly Network, Guilford, CT, USA). The phantom was made of ABS-M30 (Stratasys, Ltd.). According to Menikou *et al.* [32], the acoustic impedance of ABS-M30 was 2.13 ± 0.08 MRayl. In the imaging test (Fig. 7), the phantom was clamped in a water tank filled with degassed water. The frame rate was 25 Hz, while the update rate of the camera was a much higher 120 Hz. The probe was operated in the *bladder* mode with an imaging depth of 9 cm and a gain of 65%. The probe was fixed 22 ± 2 mm above the highest point of the phantom. Based upon the width of the phantom, the probe was translated 50 mm along x-axis of the camera, from the left to right side of the phantom. The 2D ultrasound frame was capture every 0.2 mm. Therefore, 250 frames were captured along with the motion data. Translational tracking accuracy was assessed by comparing each recorded step with the predefined one. Since the probe was translated along one direction, the other five degree-of-freedom were set as constant values for a better reconstruction. The frames were then stacked based upon the tracked position using MATLAB and the tracking volume was then reconstructed.

IV. RESULTS

A. Single-Axis Rotational Tracking Performance

Table I and Table II summarize the overall tracking performance during single-axis rotation. The stepper motor was set to rotate one revolution at a time in each test. The recorded rotation was the measurement of the rotational angle from the camera. The difference was defined as the error between the initial and final angle readings. Thus, the ground truth for

TABLE II

MEAN MISSING DATA PERCENTAGE OF SINGLE-AXIS ROTATION

	X-axis	Y-axis	Z-axis	Mean
2D	21.37%	16.61%	100%	45.99%
HS	0.06%	0.23%	0.43%	0.24%

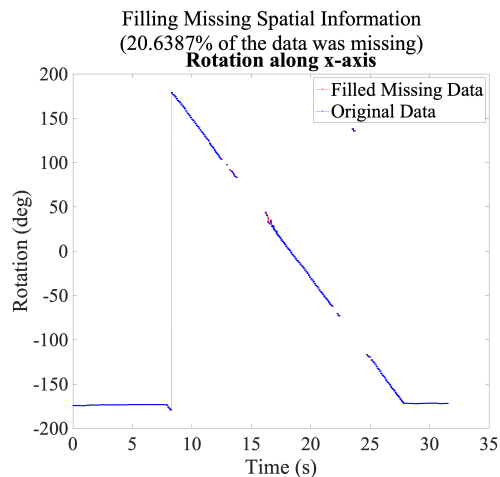
the recorded rotation and difference should be 360° and 0° , respectively. In addition, as mentioned in the previous section, a 2D marker rigid body greatly limited the rotational range of the probe operation. When the probe exceeded the allowed range, the camera no longer recognized the whole rigid body; to avoid adding bias or noise, no motion data was recorded at that time. Accordingly, the tracking performance of the hemispherical marker rigid body in this study was evaluated based on the missing data percentage, defined by the following equation.

$$\text{Missing Data Percentage (\%)} = \frac{n_{\text{missing}}}{n_{\text{total}}} \times 100\% \quad (4)$$

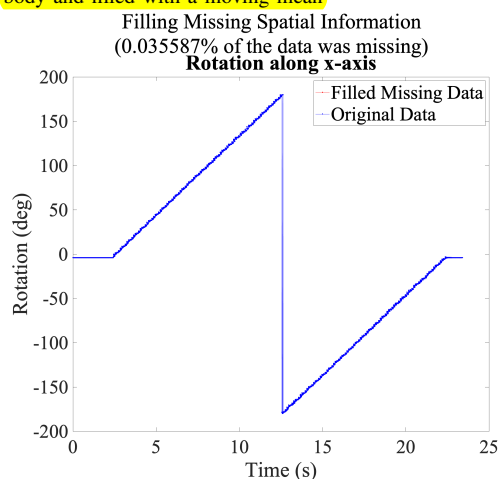
Where: n_{missing} is the number of missing data points and n_{total} is the number of total data points. The test results shown in Table I indicated two similar tracking accuracy and Table II demonstrated significant improvement in tracking robustness by the hemispherical marker rigid body. A missing data percentage of 100% in Table II means that the rotational tracking along the z-axis was completely disabled while using the 2D marker rigid body. This was because when rotating about the z-axis, the marker rigid body plane was always perpendicular to the image plane of the camera. In this scenario, all the five markers were colinear and the rigid body created could not be identified by the camera no matter at what angle. Similarly, when rotating about x-axis and y-axis, there was a rotational range where the markers were considered colinear by the camera. Thus, the missing data percentage was much higher than that of the hemispherical marker rigid body. A higher missing data percentage means less accurate tracking and harder to interpolate with a moving mean method. Fig. 6(a) showed one sample case of tracking the single-axis rotation using the 2D marker rigid body. In this case, 20.64% of the data was missing and only a few data samples could be filled with the window length of 12 sample data points; some remained missing due to inadequate neighboring entries. However, with the hemispherical marker rigid body attached, only 1 data point out of 2810 total data points were lost. Therefore, the motion plotted in Fig. 6(b) was more reliable and the missing data points could be easily filled.

B. Single-Axis Translational Tracking Performance

As mentioned in the previous section, the probe was translated at a step of 0.2 mm. In total, 249 steps of translation were made to translate the probe from the left side of the phantom to the right. When the camera was placed 1.92 m away from the phantom at the same height, the averaged measured step was 0.1902 mm, indicating the tracking system had acceptable tracking performance with an averaged error of 9.8×10^{-3} mm in this experiment setting. A histogram shown in Fig. 8 was plotted and a normal density function



(a) 20.64% of the data was missing using the 2D marker rigid body and filled with a moving mean



(b) 0.04% of the data was missing using the hemispherical marker rigid body and filled with a moving mean

Fig. 6. Missing data filled with a moving window length of 12 sample data points

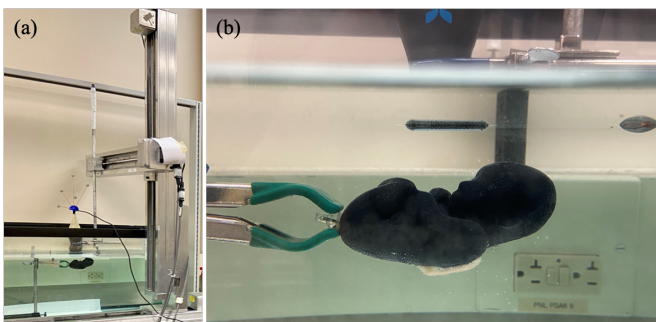


Fig. 7. Imaging test setup. (a) The probe was held and translated by a linear motion stage; (b) The phantom was clamped in a water tank with the probe held above.

was then fitted to further demonstrate the distribution. From the distribution, 77.91% of the measured steps were located from 0.15 mm to 0.25 mm, with only 3 outliers less than 0.12 mm and 3 outliers larger than 0.3 mm. The variance of the tracked step was 0.0016, which further indicated a stable tracking process.

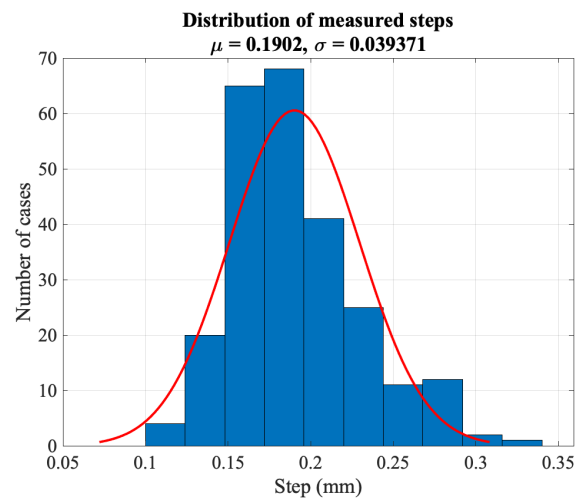


Fig. 8. Histogram of steps from the imaging test. Most steps ($\sim 77.91\%$) were captured by the tracking system located in the range of $[0.15, 0.25]$; the averaged measured step was 0.1902 mm.

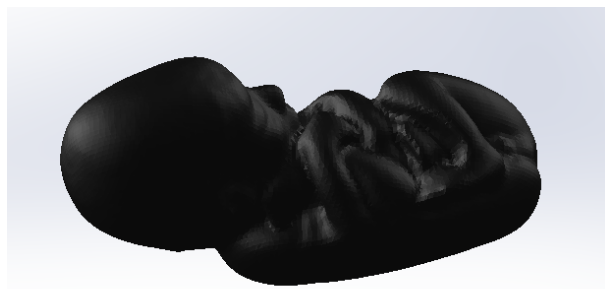
C. Imaging Test with a 4-Month Fetal Phantom

An imaging test with a 4-month fetal phantom was conducted to demonstrate the volume reconstruction performance with enhanced ultrasound probe tracking using the designed hemispherical marker rigid body. The volume reconstruction in freehand 3D ultrasound is achieved by specifying the position and orientation of each B-scan image [33] in the reconstruction volume. Thus, the reconstruction quality depends both on tracking accuracy as well as continuity of the collected data. And in terms of continuity of the collected data, tracking with 2D marker rigid body can lose tracking of the trajectory up to a few seconds due to marker occlusion so that the generated frames cannot be inserted into the volume. Fig. 9(a) demonstrates the fetal phantom that was used for the volume reconstruction. Comparing Fig. 9(b) with Fig. 9(a), the upper surface of the reconstructed phantom was clearly displayed. By rotating the reconstructed volume, the forehead, arms and the femurs of the phantom could be viewed without mentally combining the frames to imagine the structure. This reconstruction verified that despite an averaged missing data percentage of 0.36%, the collected motion data was enough to reconstruct the target volume.

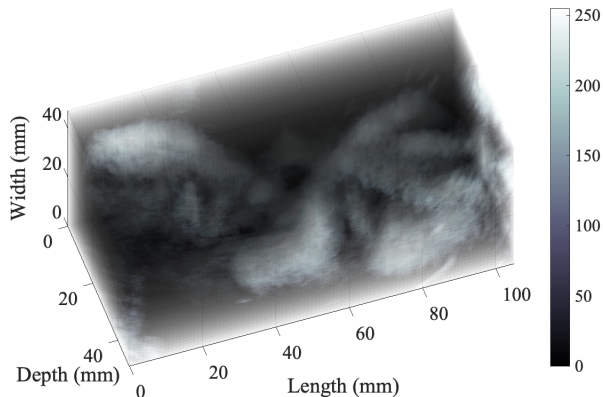
In addition, similar to the special case of collinear fiducials discussed in [34], many commercial marker rigid bodies with collinear fiducials cause failures in registration due to no unique solution. As discussed in this study, when 2D rigid body is perpendicular to camera lens, the visible markers are collinear in the camera's view. Thus, a big portion of data (up to 41.54% in the lab tests) will be missing in such cases and causes the corresponding frames unable to insert in the reconstruction volume. And no unique solution to registration can be another serious issue on registration, reconstruction and visualization.

V. DISCUSSION AND CONCLUSIONS

In this study, we constructed a printable hemispherical rigid body with 13 holes to accommodate passive retro-reflective



(a) 3D Model of the printed phantom



(b) Reconstructed phantom from the 2D ultrasound frames

Fig. 9. Volume reconstruction of a 3D printed phantom

markers. This configuration allowed successful camera-based tracking of a 360° rotation with little data missing, which improving both the tracking accuracy and (by a significant margin) the rotational range based on the test results. With markers attached to the rigid body and proper rod lengths connecting the markers to the rigid body, users can create an asymmetric and optimized distributed marker layout for their tracking purposes. A non-coplanar marker layout performs more robustly during the 3D freehand ultrasound exam compared with the 2D marker rigid body. In this study, on average, 99.76% of the rotational motion information was recorded during the tracking with the hemispherical marker rigid body, while only 54.01% on average was captured using the coplanar marker configuration. With data post-processing, it is easier to fill the missing data provided when the missing data percentage is small, which occurs with the hemispherical marker rigid body. Future work includes reducing the size of the hemispherical rigid body so that the small markers are less likely to be hidden by the marker rigid body. An algorithm to automatically generate the marker layout is also vital to making the design more practical and user-friendly. Additional tests with freehand ultrasound operation should be conducted in clinical settings to verify the feasibility of this camera-based tracking system along with the designed marker rigid body.

REFERENCES

- [1] S. R. Ghorayeb, W. Lord, and S. S. Udpa, "Application of a beamforming technique to ultrasound imaging in nondestructive testing," *IEEE transactions on ultrasonics, ferroelectrics, and frequency control*, vol. 41, no. 2, pp. 199–208, 1994.
- [2] T. L. Szabo, *Diagnostic ultrasound imaging: inside out*. Academic Press, 2004.
- [3] M. Hansmann, B.-J. Hackelöer, and A. Staudach, *Ultrasound diagnosis in obstetrics and gynecology*. Springer Science & Business Media, 2012.
- [4] M. Abdolnabehjad Bahramabadi, "Sensorless out-of-plane displacement estimation for freehand 3D ultrasound applications," Ph.D. dissertation, Carleton University, 2014.
- [5] F. Mohamed and C. V. Siang, "A survey on 3D ultrasound reconstruction techniques," in *Artificial Intelligence-Applications in Medicine and Biology*. IntechOpen, 2019.
- [6] M.-A. Janvier, S. Merouche, L. Allard, G. Soulez, and G. Cloutier, "A 3-D ultrasound imaging robotic system to detect and quantify lower limb arterial stenoses: in vivo feasibility," *Ultrasound in medicine & biology*, vol. 40, no. 1, pp. 232–243, 2014.
- [7] K. Baba, K. Satoh, S. Sakamoto, T. Okai, and S. Ishii, "Development of an ultrasonic system for three-dimensional reconstruction of the fetus," *Journal of Perinatal Medicine-Official Journal of the WAPM*, vol. 17, no. 1, pp. 19–24, 1989.
- [8] Q. Huang and J. Lan, "Remote control of a robotic prosthesis arm with six-degree-of-freedom for ultrasonic scanning and three-dimensional imaging," *Biomedical Signal Processing and Control*, vol. 54, p. 101606, 2019.
- [9] J. T. Yen, J. P. Steinberg, and S. W. Smith, "Sparse 2-D array design for real time rectilinear volumetric imaging," *IEEE transactions on ultrasonics, ferroelectrics, and frequency control*, vol. 47, no. 1, pp. 93–110, 2000.
- [10] I. O. Wygant, X. Zhuang, D. T. Yeh, O. Oralkan, A. S. Ergun, M. Karaman, and B. T. Khuri-Yakub, "Integration of 2D CMUT arrays with front-end electronics for volumetric ultrasound imaging," *IEEE transactions on ultrasonics, ferroelectrics, and frequency control*, vol. 55, no. 2, pp. 327–342, 2008.
- [11] E. Roux, E. Badescu, L. Petrusca, F. Varray, A. Ramalli, C. Cachard, M. Robini, H. Liebgott, and P. Tortoli, "Validation of optimal 2D sparse arrays in focused mode: Phantom experiments," in *2017 IEEE International Ultrasonics Symposium (IUS)*. IEEE, 2017, pp. 1–4.
- [12] A. H. Gee, R. J. Housden, P. Hassenpflug, G. M. Treece, and R. W. Prager, "Sensorless freehand 3D ultrasound in real tissue: speckle decorrelation without fully developed speckle," *Medical image analysis*, vol. 10, no. 2, pp. 137–149, 2006.
- [13] A. Lang, P. Mousavi, G. Fichtinger, and P. Abolmaesumi, "Fusion of electromagnetic tracking with speckle-tracked 3D freehand ultrasound using an unscented kalman filter," in *Medical Imaging 2009: Ultrasonic Imaging and Signal Processing*, vol. 7265. International Society for Optics and Photonics, 2009, p. 72651A.
- [14] S.-Y. Sun, M. Gilbertson, and B. W. Anthony, "Probe localization for freehand 3D ultrasound by tracking skin features," in *International Conference on Medical Image Computing and Computer-Assisted Intervention*. Springer, 2014, pp. 365–372.
- [15] R. Prevost, M. Salehi, S. Jagoda, N. Kumar, J. Sprung, A. Ladikos, R. Bauer, O. Zettinig, and W. Wein, "3D freehand ultrasound without external tracking using deep learning," *Medical image analysis*, vol. 48, pp. 187–202, 2018.
- [16] A. Chan, E. Parent, and E. Lou, "Reconstruction and positional accuracy of 3D ultrasound on vertebral phantoms for adolescent idiopathic scoliosis spinal surgery," *International journal of computer assisted radiology and surgery*, vol. 14, no. 3, pp. 427–439, 2019.
- [17] R. Finocchi, F. Aalamifar, T. Y. Fang, R. H. Taylor, and E. M. Boctor, "Co-robotic ultrasound imaging: a cooperative force control approach," in *Medical Imaging 2017: Image-Guided Procedures, Robotic Interventions, and Modeling*, vol. 10135. International Society for Optics and Photonics, 2017, p. 1013510.
- [18] X. Jiang and A. M. Al-Jumaily, "Ultrasound transducers for biomedical imaging and therapy," *Journal of Engineering and Science in Medical Diagnostics and Therapy*, vol. 1, no. 4, 2018.
- [19] T. A. Tuthill, J. Krücker, J. B. Fowlkes, and P. L. Carson, "Automated three-dimensional US frame positioning computed from elevational speckle decorrelation," *Radiology*, vol. 209, no. 2, pp. 575–582, 1998.
- [20] C. Laporte and T. Arbel, "Learning to estimate out-of-plane motion in ultrasound imagery of real tissue," *Medical image analysis*, vol. 15, no. 2, pp. 202–213, 2011.
- [21] M. Kok, J. D. Hol, and T. B. Schön, "Using inertial sensors for position and orientation estimation," *arXiv preprint arXiv:1704.06053*, 2017.
- [22] S.-h. P. Won, W. W. Melek, and F. Golnaraghi, "A Kalman/particle filter-based position and orientation estimation method using a position sensor/inertial measurement unit hybrid system," *IEEE Transactions on Industrial Electronics*, vol. 57, no. 5, pp. 1787–1798, 2009.

- [22] S.-H.-P. Won, W. W. Melek, and F. Golnaraghi, "A Kalman/particle filter-based position and orientation estimation method using a position Sensor/Inertial measurement unit hybrid system," *IEEE Trans. Ind. Electron.*, vol. 57, no. 5, pp. 1787–1798, May 2010.
- [23] A. Mahajan and M. Walworth, "3D position sensing using the differences in the time-of-flights from a wave source to various receivers," *IEEE Trans. Robot. Autom.*, vol. 17, no. 1, pp. 91–94, 2001.
- [24] S.-Y. Yeh, K.-H. Chang, C.-I. Wu, H.-H. Chu, and J. Y.-J. Hsu, "GETA sandals: A footstep location tracking system," *Pers. Ubiquitous Comput.*, vol. 11, no. 6, pp. 451–463, Aug. 2007.
- [25] Z. Zhou, B. Wu, J. Duan, X. Zhang, N. Zhang, and Z. Liang, "Optical surgical instrument tracking system based on the principle of stereo vision," *J. Biomed. Opt.*, vol. 22, no. 6, Jun. 2017, Art. no. 065005.
- [26] A. Medien, "Implementation of a low cost marker based infrared optical tracking system," M.S. thesis, Hochschule Median, Fachhochschule Stuttgart, Stuttgart, Germany, 2006.
- [27] M. A. Hamid, J. Beers, and M. Omar, "Extracting depth information using a correlation matching algorithm," *JSEA*, vol. 5, no. 5, pp. 304–313, 2012.
- [28] M. Schlegel *et al.*, "Predicting the accuracy of optical tracking systems," Ph.D. dissertation, Inst. Strömungsmechanik Technische Akustik, Technische Univ. Berlin MB1, Citeseer, Princeton, NJ, USA, 2006.
- [29] A. D. Wiles, D. G. Thompson, and D. D. Frantz, "Accuracy assessment and interpretation for optical tracking systems," *Proc. SPIE*, vol. 5367, pp. 421–432, May 2004.
- [30] J. Wang, L. Qi, and M. Q.-H. Meng, "Robot-assisted occlusion avoidance for surgical instrument optical tracking system," in *Proc. IEEE Int. Conf. Inf. Autom.*, Aug. 2015, pp. 375–380.
- [31] Q. Cai, C. Peng, J. C. Prieto, A. J. Rosenbaum, J. S. A. Stringer, and X. Jiang, "A low-cost camera-based ultrasound probe tracking system: Design and prototype," in *Proc. IEEE Int. Ultrason. Symp. (IUS)*, Oct. 2019, pp. 997–999.
- [32] G. Menikou and C. Damianou, "Acoustic and thermal characterization of agar based phantoms used for evaluating focused ultrasound exposures," *J. Therapeutic Ultrasound*, vol. 5, no. 1, p. 14, Dec. 2017.
- [33] M. H. Mozaffari and W.-S. Lee, "Freehand 3-D ultrasound imaging: A systematic review," *Ultrasound Med. Biol.*, vol. 43, no. 10, pp. 2099–2124, Oct. 2017.
- [34] J. B. West and C. R. Maurer, "Designing optically tracked instruments for image-guided surgery," *IEEE Trans. Med. Imag.*, vol. 23, no. 5, pp. 533–545, May 2004.



Qianqian Cai (Student Member, IEEE) received the B.S. degree in mechanical engineering from North China Electric Power University, Beijing, China, in 2016, and the M.S. degree in mechanical engineering from North Carolina State University, Raleigh, NC, USA, in 2018.

She currently works as a Research Assistant under Dr. Xiaoning Jiang's supervision at the Micro/Nano Engineering Laboratory, North Carolina State University. Her research involves ultrasound probe tracking and intelligent 3-D freehand ultrasound applications.



Chang Peng (Member, IEEE) received the Ph.D. degree in mechanical engineering from the University of Florida, Gainesville, FL, USA, in 2018, with a focus on developing ultrasonic transducers for direct-contact ultrasonic fabric drying.

He is currently a Postdoctoral Research Scholar with the Micro/Nano Engineering Laboratory, North Carolina State University, Raleigh, NC, USA, working on the design and fabrication ultrasonic transducers for sensing, imaging, and therapy applications.



Jian-Yu Lu (Fellow, IEEE) received the B.S. degree in electrical engineering from Fudan University, Shanghai, China, in February 1982, the M.S. degree in acoustics from Tongji University, Shanghai, China, in 1985, and the Ph.D. degree in biomedical engineering from Southeast University, Nanjing, China, in 1988.

From December 1988 to February 1990, he was a Postdoctoral Research Fellow with the Mayo Medical School (MMS), Rochester, MN, USA. Since 1997, he has been a Professor with

the Department of Bioengineering, The University of Toledo (UT), Toledo, OH, USA. Since 1998, he has been an Adjunct Professor with the UT College of Medicine and Life Sciences. Before joining UT as a Professor in 1997, he was an Associate Professor of biophysics at MMS and an Associate Consultant at the Department of Physiology and Biophysics, Mayo Clinic/Foundation, Rochester.

Dr. Lu was a fellow of the American Institute of Ultrasound in Medicine (AIUM) in 2005 and the American Institute for Medical and Biological Engineering (AIMBE) in 2007. He served as the President for the IEEE Ultrasonics, Ferroelectrics, and Frequency Control Society (UFFC-S) from 2014 to 2015, the Editor-in-Chief for the IEEE TRANSACTIONS ON ULTRASONICS, FERROELECTRICS, AND FREQUENCY CONTROL (TUFFC) from 2002 for six years, the General Chair of the 2008 IEEE International Ultrasonics Symposium (IUS) that was held in Beijing, China, and the Technical Program Committee (TPC) Chair of the 2001 IEEE IUS held in Atlanta, GA, USA, in addition to serving on many other leadership positions in UFFC-S. He received the 2016 Distinguished Service Award from the UFFC-S and the Outstanding TUFFC Paper Award for two papers from the UFFC-S in 1992.



Juan C. Prieto received the M.S. and Ph.D. degrees from the National Institute of Applied Sciences of Lyon, Lyon, France, in 2010 and 2014, respectively.

His current work in obstetrics and gynecology involves the Ultrasound Fetal Age Machine Learning Initiative (US-FAMLI), which aims to develop a low-cost obstetric ultrasound (US) for use in low- and middle-income countries (LMICs) that uses machine-learning algorithms to estimate gestational age and make diagnoses without requiring a skilled ultrasonographer. He also uses fiber tract classification using deep learning (TRAFIC), which is a fully automated tool for the labeling and classification of brain fiber tracts.



Alan J. Rosenbaum received the M.D. degree from the School of Medicine, University of Pittsburgh, Pittsburgh, PA, USA, in 2014. He completed his training in obstetrics and gynecology at The Ohio State University, Columbus, OH, USA.

He previously has worked on increasing cervical cancer screening access using low-cost HPV tests in El Salvador through the Fulbright program. He joined the Global Women's Health Division as a clinical provider and a research fellow whose primary research interest is improving access to health care through novel technologies. His current project involves the use of artificial intelligence and machine learning to improve ultrasound performance in low-resource settings in a project that has been funded by the Bill and Melinda Gates Foundation.



Jeffrey S. A. Stringer received the M.D. degree from Columbia University College of Physicians and Surgeons in 1995.

He is currently a Professor of obstetrics and gynecology with the School of Medicine, The University of North Carolina at Chapel Hill, Chapel Hill, NC, USA, and an Adjunct Professor of epidemiology with the UNC's Gillings School of Global Public Health. From 2001 to 2012, he lived in Lusaka, Zambia, where he established and led the Centre for Infectious Disease Research, Lusaka, Zambia. In 2012, he returned to Chapel Hill to lead the UNC's Division of Global Women's Health. His research focuses on birth outcomes, clinical epidemiology, and HIV in women and children. He has served as PI for over U.S. \$250 million in grant and contract funding for research, training, and technical assistance work in Africa. He currently holds active grants from the NIH, the Bill and Melinda Gates Foundation, USAID, and other sources.



Xiaoning Jiang (Senior Member, IEEE) received the B.S. degree from Shanghai Jiao Tong University, Shanghai, China, in 1990, the M.S. degree from Tianjin University, Tianjin, China, in 1992, and the Ph.D. degree from Tsinghua University, Beijing, China, in 1997. He completed his postdoctoral training at Nanyang Technological University, Singapore, from 1996 to 1997, and Pennsylvania State University, State College, PA, USA, from 1997 to 2001.

He was the Chief Scientist and the Vice President at TRS Technologies, Inc. prior to joining North Carolina State University, Raleigh, NC, USA, in 2009. He is currently a Dean F. Duncan Distinguished Professor of mechanical and aerospace engineering and a University Faculty Scholar with North Carolina State University. He is also an Adjunct Professor of biomedical engineering with North Carolina State University and The University of North Carolina, Chapel Hill, NC, USA. He is the author or the coauthor of two books, six book chapters, nine issued U.S. patents, 130 peer-reviewed journal articles, and over 100 conference papers on piezoelectric ultrasound transducers, ultrasound for medical imaging and therapy, drug delivery, ultrasound NDT/NDE, smart materials and structures, and M/NEMS.

Dr. Jiang is a member of the Technical Program Committee for a few international conferences, including the IEEE Ultrasonics Symposium (TPC-5), SPIE Smart Structures and ultrasound nondestructive evaluation (NDE), The American Society of Mechanical Engineers International Mechanical Engineering Congress & Exposition (ASME IMECE), the Institute of Electrical and Electronics Engineers International Conference on Nanotechnology (IEEE NANO), and the Institute of Electrical and Electronics Engineers Nanotechnology Materials and Devices Conference (IEEE NMDC). He is also a fellow of the ASME and the Society of Photo-optical Instrumentation Engineers (SPIE). He is also the NanoAcoustics Technical Committee Chair of the Institute of Electrical and Electronics Engineers Nanotechnology Council (IEEE NTC). He was a Distinguished Lecturer of IEEE NTC from 2018 to 2019, an Editorial Board Member of the *Sensors* journal, a Senior Associate Editor of the *ASME Journal of Engineering and Science in Medical Diagnostics and Therapy*, and the Co-Editor-in-Chief of *IEEE Nanotechnology Magazine*.